Environmental Science & Technology

Article

pubs.acs.org/est

Direct Photolysis of α-Pinene Ozonolysis Secondary Organic Aerosol: Effect on Particle Mass and Peroxide Content

Scott A. Epstein, Sandra L. Blair, and Sergey A. Nizkorodov*

Department of Chemistry, University of California, Irvine, California 92697, United States

Supporting Information

ABSTRACT: Primary and secondary organic aerosols (POA and SOA) contain a complex mixture of multifunctional chemicals, many of which are photolabile. Much of the previous work that aimed to understand the chemical evolution (aging) of POA and SOA has focused on the reactive uptake of gas-phase oxidants by particles. By stripping volatile compounds and ozone from α-pinene ozonolysis SOA with three 1-m-long denuders, and exposing the residual particles in a flow cell to near-ultraviolet (λ>300 nm) radiation, we find that condensed-phase photochemistry can induce significant changes in SOA particle size and chemical composition. The particle-bound organic peroxides, which are highly abundant in α-pinene ozonolysis SOA (22 ± 5% by weight), have an atmospheric photolysis lifetime of about 6 days at a 24-h average solar zenith angle (SZA) of 65° experienced at 34° latitude (Los Angeles) in the summer. In addition, the particle diameter shrinks 0.56% per day under these irradiation conditions as a result of the loss of volatile photolysis products. Experiments with and without the denuders show similar results, suggesting that condensed-phase processes dominate over heterogeneous reactions of particles with organic vapors, excess ozone, and gas-phase free radicals. These condensed-phase photochemical processes occur on atmospherically relevant time scales and should be considered when modeling the evolution of organic aerosol in the atmosphere.

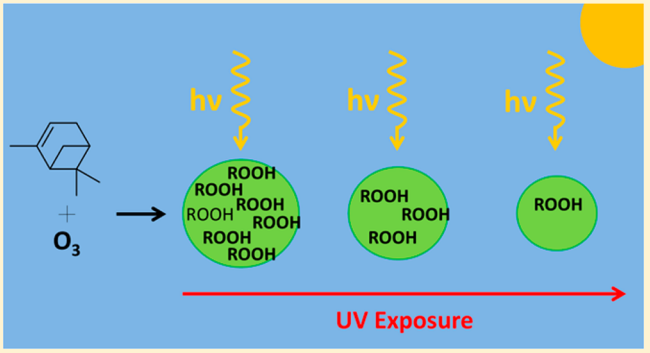

INTRODUCTION

Atmospheric particulate matter (PM) is ubiquitous, causes adverse health effects, alters climate, and degrades visibility. Depending on location, organic compounds contribute 20 to 80% of the total nonrefractory PM mass smaller than 1 μm in diameter.[1] In order to understand the environmental impact of this organic aerosol (OA), we must comprehensively account for all chemical aging processes that affect the chemical composition, concentration, and physical properties of organic particles. The majority of past OA aging studies have focused on photooxidation driven by gas-phase and heterogeneous reactions of gas-phase oxidants with OA constituents and gas-phase photochemistry.[2] However, UV radiation from the sun can induce photolysis and other photochemical reactions of oxygenated organic compounds directly in the condensed organic aerosol phase.[3] Gas-phase photolysis of volatile organic compounds is well studied and is accounted for in atmospheric models. On the contrary, changes in OA composition and concentration arising from condensed-phase photolysis of low-volatility organic compounds have not been thoroughly quantified. OA contains peroxides,[4,5] carbonyls,[6] organonitrates,[6] and other photolabile compounds that absorb light at actinic wavelengths. UV radiation is capable of reaching every molecule in a typical particle as opposed to heterogeneous photooxidation, which may be limited by mass transfer to surface reactions, especially in glassy aerosols.[7] (Only coarse particles that are dominated by highly absorbing species such as black carbon may absorb UV to the extent that it does not reach every molecule in the particle.)

Previous studies have found evidence of UV light modifying the composition and properties of organic aerosol. Presto et al.[8] found that the formation of α-pinene ozonolysis secondary organic aerosol (SOA) in a smog chamber was suppressed by 20−40% when exposed to UV light. Various gas-phase photodegradation products were identified with sensitive detection techniques after irradiating d-limonene ozonolysis SOA collected on substrates.[9−11] Walser et al.[11] suggested that peroxides are the primary UV absorbers in d-limonene ozonolysis SOA based on the shape of its photodissociation action spectrum (the relative amount of gas-phase photolysis products produced as a function of the UV photolysis wavelength). Kroll et al.[12] observed initial SOA growth during the irradiation of a mixture of isoprene and hydrogen peroxide under low-NOx conditions, followed by a decrease in particle size as the SOA mixture was continuously irradiated. However, low-NOx β-pinene SOA particles did not shrink upon irradiation, indicating that a rapid loss of SOA mass under

Received: May 12, 2014
Revised: August 26, 2014
Accepted: August 28, 2014
Published: August 28, 2014

   dx.doi.org/10.1021/es502350u | Environ. Sci. Technol. 2014, 48, 11251−11258

UV exposure is dependent on the chemical composition of the SOA. Surratt et al.[5] detected similar decreases in the particle size of low-NOx isoprene SOA upon irradiation. Iodometric methods indicated that the organic peroxide content of the SOA decreased significantly during irradiation. Since the experiments of Kroll et al.[12] and Surratt et al.[5] were performed in a chamber, the authors were unable to rule out changes in particle composition and concentration due to the effects of OH radical reactions or repartitioning arising from the irradiation of gas-phase species.

Observations of aerosol photolysis in any chamber experiment are complicated by the interaction of particles and organic vapors and by the photochemical recycling of oxidants. Irradiation of particles collected on substrates[9−11] or in aqueous extracts[13,14] eliminates interference from gas-phase oxidants and volatiles but may introduce additional complexities that are not applicable to the atmosphere. For example, volatile products formed during irradiation of bulk SOA materials and solutions may be inhibited from evaporation by mass-transfer limitations. To overcome these limitations, we designed a coupled smog-chamber-flow tube approach in which SOA is irradiated without the presence of gas-phase oxidants and high-volatility organic gases. We conducted a series of experiments with α-pinene ozonolysis SOA using this setup. Along with tracking particle size, mass concentration, and chemical composition as a function of irradiation time, we also quantified changes in the overall peroxide content of the SOA. Organic peroxides are a significant component in SOA; for example, as much as 50% by weight of α-pinene ozonolysis SOA mass was previously attributed to organic peroxides.[4] We similarly observe high peroxide content (22 ± 5% by weight) in α-pinene ozonolysis SOA, which is depleted by condensed-phase irradiation over atmospherically relevant time scales. In addition, aerosol size measurements reveal slight changes in particle diameter during irradiation, which imply that condensed-phase photochemical processes result in a net loss of organic mass from particles.

MATERIALS AND METHODS

Due to space constraints, some of the experimental details have been delegated to the Supporting Information (Figures S1−S9). Only the most essential experimental details are reported below.

Case Studies A−C: Effect of Irradiation on Particle Composition and Size with and without High-Volatility Vapors and Oxidants. Experiments were conducted using two different setups. In the first set of experiments (Figure 1A), we used a single quartz flow cell to irradiate α-pinene ozonolysis SOA, which was made in a 6 m^3 Teflon smog chamber. In each experiment, 125 ppb (part per billion by volume) of α-pinene (Alpha-Aesar 98%) was reacted in the dark with 400 ppb of ozone produced with a commercial ozone generator. We measured the particle concentration and chemical composition with a Scanning Mobility Particle Sizer (SMPS, TSI 3080 Electrostatic Classifier and TSI 3775 or 3776 Condensation Particle Counter) and an Aerodyne Time-of-Flight Aerosol Mass Spectrometer (ToF-AMS), respectively. Concentrations of specific gas-phase compounds were measured with an Ionicon Proton Transfer Reaction Time-of-Flight-Mass Spectrometer (PTR-ToF-MS). After the particle mass concentration in the chamber stabilized, the SOA was drawn at 0.39 L/min through three 1-m-long denuders that consisted of an inner and outer tube with activated charcoal in the annulus.

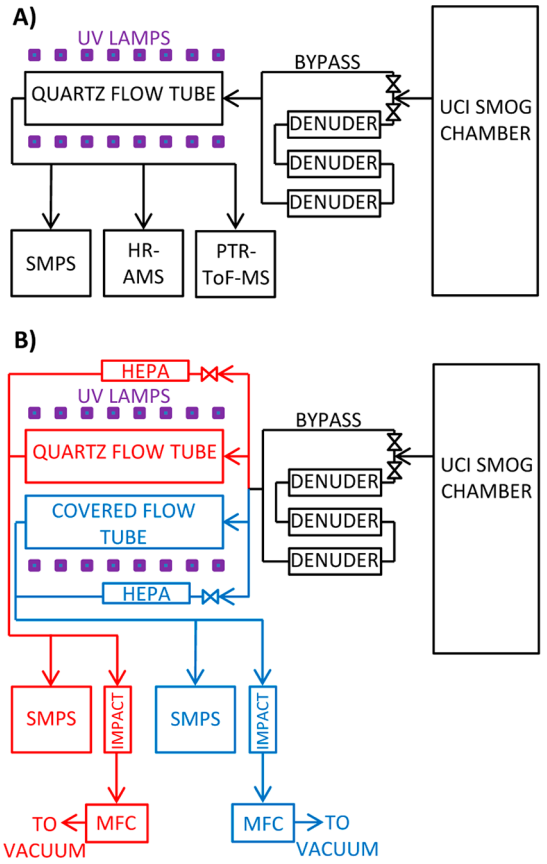

Figure 1. (A) Experimental setup to observe changes in particle composition and concentration upon UV exposure. (B) Experimental setup used to determine changes in particle median mobility-equivalent diameter and peroxide content as a function of irradiation time.

The residence time in the denuders (3.5 min) was sufficient to remove all of the unreacted ozone (see Figure S1) and the majority of the gas-phase compounds (see Figure S2). A three-way valve was used to switch between the train of denuders and a bypass line. The aerosol was then drawn into a 24 L quartz flow tube (7″ outer diameter) surrounded by 16 UV lamps (Phillips 20W Ultraviolet B TL 20W/01 RS) in a vented protective enclosure. The wavelength dependence of light produced by these lamps is shown in Figure S5; it is dominated by a strong emission line at ∼312 nm. Actinometry experiments, which are described in the Supporting Information, were used to determine the scaling factor (E = 414 ± 30; see eq S4) between the SOA photolysis rate inside the quartz flow tube and that in the ambient atmosphere. Isopropyl nitrite, with its known quantum yield and absorption cross section,[15] was used as the actinometer. The calibrated photon flux inside the flow tube was then used to calculate the effective photolysis rate experienced by SOA when exposed to 24-h averaged sunlight in Los Angeles on the summer solstice. The SMPS, ToF-AMS, and PTR-ToF-MS were positioned at the outlet of the flow tube to monitor differences in gas- and particulate-phase composition with and without UV exposure. The residence time of the SOA in the quartz flow tube was approximately 1 h, set by the sample flow rate of the instruments. Particle evaporation in the flow tube likely replenished some of the semivolatile vapors, but the vapor concentrations were expected to be lower than the gas-particle

Table 1. Summary of Experimental Conditions

case study	figure detailing setup	α-pinene [ppb]	O_3 [ppb]	denuder or bypass	added OH?	flow rate [L min^{-1}]	residence time
A	Figure 1A	125	400	denuder	no	0.39	1 h
B	Figure 1A	125	400	bypass	no	0.39	1 h
C	Figure 1A	125	400	denuder	yes	0.39	1 h
D	Figure 1B	60	100	denuder	no	0.96−6	4−25 min
E	Figure 1B	2500 + 1300	400	denuder	no	1−8	3−22 min

equilibrium values because the measured particle evaporation times for α-pinene ozonolysis SOA (several hours)[16] are considerably longer than the flow cell residence time (1 h).

Table 1 summarizes the types of experiments conducted with this setup. In case study A, we generated SOA in the smog chamber, passed it through the denuder train, and drew it through the flow tube. The SMPS, ToF-AMS, and PTR-ToF-MS sampled the SOA with and without the presence of UV-light. In case study B, SOA was generated in the smog chamber, sent through the bypass line around the denuder train, and drawn through the flow tube. The same series of perturbations in UV exposure were conducted. Case study C was conducted to investigate the effects of irradiating SOA with a higher average oxidation state. α-Pinene SOA was generated in the chamber and subsequently aged with additional OH radical production from 2,3-dimethyl-2-butene (TME) ozonolysis (Sigma-Aldrich ≥99%) in the dark.[17] TME was added to the chamber by evaporation of the headspace above a column of TME at a rate of 50 μg min^{-1} over 90 min. The ozone concentration was reduced linearly at a rate of 2 ppb min^{-1} due to its reaction with TME. The resulting aerosol mixture was passed through the denuder train and drawn through the flow tube where we subjected it to perturbations in UV exposure.

Case Study D: Measurements of Aerosol Size as a Function of Irradiation Time. A parallel dark flow tube was added to conduct the second set of experiments at variable flow rates (Figure 1B). With this setup, we were able to vary the flow rate and residence time through the flow tubes independently of the sampling instruments. To observe how particle diameter changes with UV exposure, we reacted 60 ppb of α-pinene with 100 ppb of ozone in the smog chamber (case study D in Table 1). The resulting aerosol was passed through the denuder system, split into two flows, and drawn through each of the flow cells. Mass flow controllers were used to govern the residence time of the SOA in each of the flow tubes. The UV lights remained on throughout the experiment but only penetrated the walls of the quartz flow tube (the control flow tube was protected from radiation with a layer of foil). An SMPS was used to obtain particle size data as a function of aerosol residence time in the quartz flow tube. A second SMPS was used to monitor particle size in the dark flow cell. This dual SMPS measurement allowed us to sensitively track small changes in median mobility-equivalent diameter at various UV-exposure times.

Case Study E: Measurements of Aerosol Peroxide Content as a Function of Irradiation Time. We also conducted experiments designed to measure changes in SOA peroxide content as a function of UV exposure with an iodometric peroxide test originally developed by Banerjee and Budke.[18] Several researchers have used versions of this test to determine peroxide content in aerosols.[4,5,13,19,20] Experimental details and several important considerations when using this test are summarized in Mutzel et al.[21] Since the iodometric test's sensitivity is limited, it was necessary to do experiments at significantly higher SOA concentrations. In these experiments, 2.5 ppm of α-pinene was reacted in the dark with 400 ppb of ozone (case study E in Table 1). After allowing the mixture to react for 30 min, we added an additional 1.3 ppm of α-pinene to consume the excess ozone and quench the reaction. One hour later, the SOA was drawn through the light and dark flow tubes at flow rates ranging from 1 to 7 L min^{-1} and collected with two SKC Sioutas Cascade Impactors.[22] Stage "A" (>2.5 μm) of the impactors was used to retain any fugitive charcoal dust from the denuders before it reached the substrate. Stage "D" (>0.25 μm) was used to impact approximately 10−20% of the SOA particles on the foil substrate. The residence time in the flow cells was modified with two calibrated mass flow controllers. Two bypass lines with in-line HEPA filters were used as "make-up" air flow to maintain a constant 7 L min^{-1} flow through the impactors at any residence time. This "make-up" flow through the HEPA filters (Figure 1B) laden with the SOA vapor-phase ensured that we did not perturb the partitioning of the collected particles while still maintaining a constant collection flow rate.

Irradiated and dark SOA was collected on aluminum foil substrates that were weighed with 1 μg precision before and after collection. Collection times were dependent on the selected aerosol flow rate through the flow tubes but were set to collect approximately 40 μg of SOA on each of the foil substrates. We then dissolved each sample in a small aliquot (several mL) of a solution containing 350 μL of glacial acetic acid (EMD 99.7%) and 25 mL of methanol (Sigma-Aldrich Absolute acetone free) in 100 mL of deionized water. The aliquot volume was selected as to generate a SOA mass concentration of 5.7 μg mL^{-1}. Three 2 mL aliquots were withdrawn from each of the irradiated and dark solutions. We then purged each solution in a septum-cap vial with nitrogen gas (Airgas UHP-300) to eliminate the dissolved oxygen. After 5 min of purging, we added 100 μL of 1.20 M potassium iodide (Fisher Scientific 99.7%) solution. Each solution was allowed to develop in a gastight vial for 5 h. The long reaction time was necessary because the measured I_3^- concentration continued to increase until it stabilized after approximately 5 h of reaction time; we wanted to ensure that the reaction was at least 95% complete before each measurement was taken. A UV−vis spectrometer (Shimadzu UV-2450) was used to measure the absorbance of each sample at 351 nm as suggested by Mutzel et al.[21] Calibration solutions prepared by the dilution of 3.0% hydrogen peroxide (concentration verified by taking absorption spectrum) were used to validate this method yielding an I_3^- extinction coefficient of 26 710 M^{-1} cm^{-1} at 351 nm in the reacted samples at concentrations between 0.18 μM and 3.5 μM peroxide. This compares well to the value of 26 400 M^{-1} cm^{-1} published in Awtrey and Connic.[23]

RESULTS AND DISCUSSION

Case Studies A−C: Effect of Irradiation on Particle Composition and Size with and without High-Volatility

Vapors and Oxidants. SMPS measurements of particle number concentration, median mobility-equivalent diameter, and mass concentration (calculated assuming a constant particle density of 1.2 g cm^{-3}) for case studies A (denuder), B (bypass), and C (added OH) are shown in Figure 2. In each

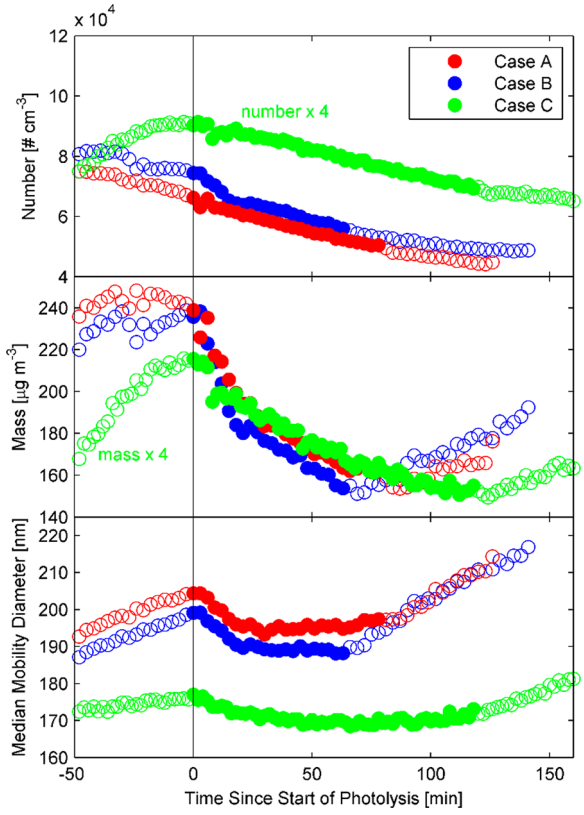

Figure 2. Number concentration, median mobility-equivalent diameter, and mass concentration estimated from the mobility measurements in the flow cell. The black line at time = 0 indicates when the lights were turned on. The points denoted with solid markers were acquired when the lights were on. Empty markers indicate that the lights were off during that point in the experiment. Lights were turned off after a different period in each of the three case studies.

of these cases, the aerosol residence time was 1 h, equivalent (eq S4) to approximately 17 ± 1.2 days of atmospheric irradiation of α-pinene SOA at a 24-h average SZA of 65° corresponding to 34° latitude (Los Angeles) at the time of the summer solstice. The number concentration exhibits a steady decline, due to particle wall losses in the smog chamber which the particles are drawn from. Turning the UV lights on or off does not noticeably change the trajectory of particle number concentration. However, the particle mass concentration clearly exhibits a decline when the lights are turned on and a slow recovery toward the initial value when the lights are turned off. The apparent mass concentration does not return to its initial value after the lights are turned off due to wall losses in the smog chamber during the experiment. Irradiation also affects the average particle size. Before the lights are turned on, median mass diameter exhibits a slow steady increase due to coagulation. Upon irradiation, the particles shrink significantly. When the lights are turned off, the median mobility-equivalent diameter grows as the irradiated particles in the flow cell are replaced by dark particles from the chamber. We attribute the observed reduction in the particle diameter and mass concentration to photochemical loss of volatile products from the irradiated particles. However, these changes could also, conceivably, result from a change in the particle density upon irradiation. Since we are not measuring the particles' density directly, we cannot estimate the relative magnitude of this effect.

Monge et al.[24] reported that particles containing suitable photosensitizers may actually increase in size when they are irradiated in the presence of VOC compounds. If this process occurred in the α-pinene ozonolysis SOA system, we would have expected to see a difference between denuded experiments (lower VOC concentrations around the particles) and undenuded experiments (higher VOC concentrations around the particles). Since we observed comparable particle shrinkage in both cases, we conclude that α-pinene ozonolysis SOA does not contain molecules that could act as efficient photosensitizers.

The ToF-AMS was used to measure aerosol composition before and after irradiation. We first verified that the small temperature increase in the flow cell resulting from the irradiation did not measurably affect the particle composition (Figure S3 and eqs S5−S13). Therefore, all of the observed changes in the particle ToF-AMS composition can be attributed to photochemistry. As expected, irradiation preferentially affects the oxygenated compounds, as the only photolabile functional groups in low NOx α-pinene SOA are carbonyls and peroxides. This preference is illustrated in Figure 3 where the fraction of

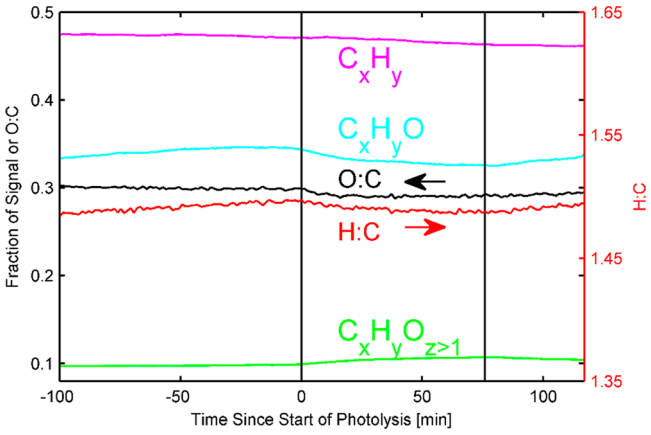

Figure 3. Fraction of signal attributed to purely hydrocarbon fragments and oxygenated hydrocarbon fragments during aerosol irradiation in case study A (the fractions do not add to 1; the remainder corresponds to fragments that do not contain carbon atoms). Average O/C corresponding to the left axis and average H/C corresponding to the right axis are also shown for the same experiment. The initial black line represents the time where the lights were turned on. The second black line indicates the time that the lights were turned off.

signal attributed to hydrocarbon fragments remains relatively constant during irradiation and the fraction of signal attributed to the oxygenated fragments evolves during irradiation.

Fragmented ions containing one oxygen atom (O1) decrease while fragmented ions with more than one oxygen increase during irradiation. The decrease in the O1 ions is larger, prompting the average O/C ratio in the SOA to drop slightly during irradiation (Figure S10). These observations may imply that the volatile products of photolysis (e.g., CO_2, H_2O, formic

dx.doi.org/10.1021/es502350u | Environ. Sci. Technol. 2014, 48, 11251−11258

acid, formaldehyde, methanol) have high oxygen content and that lower O/C compounds remaining in particles are photolyzed at a faster rate than the higher O/C compounds. However, this cannot be concluded with certainty as secondary reactions between photochemically produced free radicals and oxygen will affect the O/C in the final products.

Case studies A–C reveal similar changes in particle median mobility-equivalent diameter and mass concentration upon irradiation. In addition, changes in the average O/C ratio upon irradiation in each case were of a similar magnitude, indicating that changes in aerosol composition were alike (Figure S10). Finally, the irradiation of vapor-laden air with particles removed by a Teflon filter did not result in new particle formation in the flow tube. These observations, in combination, suggest that while the gas-phase compounds may be photolyzed, the vapor pressures of the resulting products are not low enough to induce partitioning into the condensed phase. Furthermore, the similarity of case studies A–C implies that the rates of condensed-phase photochemical processes must be higher than the rates of heterogeneous reactions between photochemically produced gas-phase radicals and particles.

Case Studies D and E: Dual-Flow Cell Experiments. After modification of the experimental apparatus to include a dark flow cell along with the ability to easily vary residence time in both flow cells, we were able to more accurately measure particle median mobility-equivalent diameter as a function of irradiation time. This experimental setup provided two advantages over the single-flow cell apparatus. We were able to remove the effects of SOA particle size evolution and compositional changes due to dark aging in the smog chamber by measuring both the dark and irradiated aerosol simultaneously. This allowed us to more sensitively detect small changes in particle concentration and composition with irradiation. In addition, both flow cells expose the aerosol to the same conditions except for the presence of UV light. Most importantly, the temperatures in both irradiated and control flow cells are the same, which helps compensate for any temperature-induced mass concentration changes (temperature effects on the composition are not significant to begin with Figure S3). Figure 4 illustrates the effect of UV exposure on the median particle mobility-equivalent diameter for SOA generated from the reaction of 60 ppb of α-pinene with 100 ppb of ozone (25 μg m^{-3} of SOA).

To illustrate changes in median mobility-equivalent diameter during irradiation on an atmospherically relevant time scale, a secondary red axis illustrates the corresponding residence time at a SZA of 65°, which corresponds to the 24-h average SZA at 34° latitude (Los Angeles) on the summer solstice. The median mobility-equivalent diameter in both the dark and UV-exposed flow cell was tracked continuously with separate SMPS instruments. Dark experiments (shown as the three values when τ = 0) were used to calibrate the measurements from each flow cell with each other. The median mobility-equivalent diameter shrinks measurably as the SOA is irradiated. In the absence of a complete understanding of the kinetic processes that will govern a decrease in median mobility-equivalent particle size, we empirically fit the decay with a linear function. The median mobility-equivalent diameter decays at a rate of 0.56 ± 0.06% per day at a SZA of 65°. The right y-axis in Figure 4 shows how irradiation time affects the geometric standard deviation of the particle size. At longer irradiation times, the particle distribution becomes broader and shifts to smaller sizes.

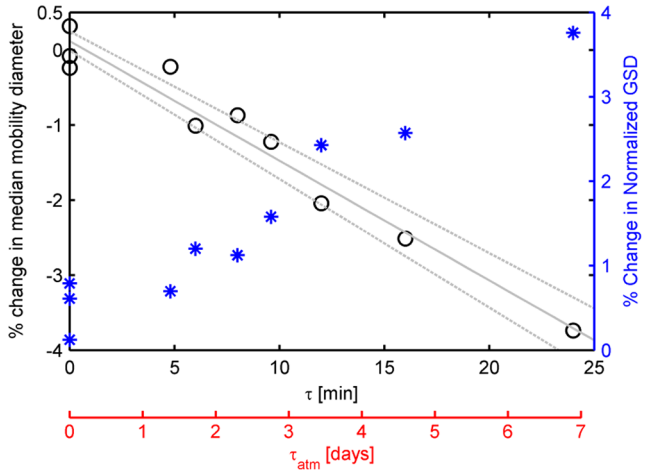

Figure 4. Change in median mobility-equivalent diameter as a function of aerosol residence time inside the flow cell (left y-axis). The percent change in the geometric standard deviation—between the dark and light flow cell—normalized by the median mobility-equivalent diameter is shown on the right y-axis. The red x-axis, τ_{atm}, shows the corresponding atmospheric irradiation time at a solar zenith angle of 65°. The gray line is a linear-least-squares fit of the data. Dash gray lines indicate the bounds of the fit considering the uncertainty in the fitting constants.

With offline iodometric peroxide tests, we were able to quantify the change in peroxide content as a function of irradiation time. The average peroxide content in the absence of irradiation was (7.9 ± 1.7) × 10^{-4} mol peroxide per gram SOA. With an assumed average molecular weight of 273 g mol^{-1} (estimated from unpublished high-resolution mass-spectrometry data), this corresponds to a 22 ± 5% weight fraction of peroxides in SOA, or equivalently to 8.5 ± 1.8% of oxygen atoms residing in the peroxy bonds. This value is significantly smaller than the one measured by Docherty et al.[4] (~47% with a similar assumed molecular weight of 300 g mol^{-1}). The disagreement may be due to differences in SOA preparation.

The normalized molar fraction of peroxide remaining in a sample as a function of irradiation time is presented in Figure 5.

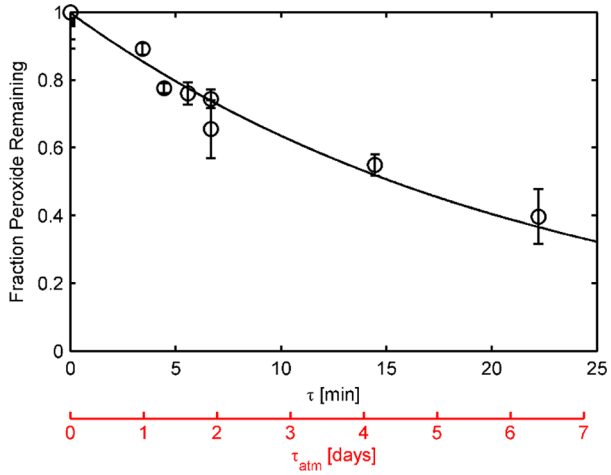

Figure 5. Fraction of peroxide remaining on a molar basis [moles remaining after UV exposure/mol present before UV exposure] in SOA after exposure to UV light. Exposure to laboratory UV light is shown on the black x-axis. The red x-axis shows the corresponding atmospheric irradiation time at a solar zenith angle of 65°.

dx.doi.org/10.1021/es502350u | Environ. Sci. Technol. 2014, 48, 11251–11258

Each data point is the result of averaging three peroxide tests of the same SOA sample. A first-order fit of the data yields a lifetime of 6.3 ± 0.6 days at SZA = 65°. Note that the spontaneous decomposition of peroxides, which could occur in the absence of UV light, is explicitly accounted for in these experiments as we compare the peroxide content in the irradiated flow cell to the peroxide content in the dark flow cell. These experiments measure the net loss in peroxide content. Because peroxide photolysis may lead to the formation of secondary peroxides, the primary photochemical reactions may occur at faster rates than the measured lifetime would suggest.

Measurements of chemical composition and particle size suggest that photolysis is destroying particle-bound peroxides, which is consistent with the relatively weak and highly photolabile nature of O−O peroxide bonds. Alkoxyl (RO) and hydroxyl (OH) radicals formed by the photolysis of peroxides could lead to secondary reactions in the condensed phase. These reactions could further functionalize neighboring SOA molecules and result in a decrease in vapor pressure. However, the observed particle shrinkage during irradiation suggests that fragmentation, leading to the production of volatile products, wins over the functionalization. The predominance of fragmentation is consistent with a recent study by Hung et al.,[25] who observed an efficient photodegradation of films of α-pinene ozonolysis secondary organic material upon 254 nm photolysis and suggested that aging by ultraviolet radiation was likely due to the presence of organic hydroperoxides in the film. Most likely, the two radicals formed from peroxide decomposition do not have a chance to escape the "solvent cage" of the organic matrix (indicated by square brackets in the equations below) and either recombine or disproportionate[26] within the cage:

$$\mathrm{ROOR'} + h\nu \rightarrow [\mathrm{RO} + \mathrm{R'O}] \rightarrow \text{carbonyl} + \text{alcohol} \quad (1)$$

$$\mathrm{ROOH} + h\nu \rightarrow [\mathrm{RO} + \mathrm{OH}] \rightarrow \text{carbonyl} + \mathrm{H_2O} \quad (2)$$

The final stable products have smaller size and higher vapor pressures than the initial peroxides and can therefore more easily evaporate from the particle. More complicated reactions, involving RO isomerization, hydrogen atom abstraction by RO from a neighboring molecule, etc., are certainly possible,[27] but they are also expected to lead to products that are on average smaller in size than the original peroxides. This result is consistent with the previous observation of the fragmentation of oligomeric SOA compounds and formation of volatile products in bulk SOA irradiation experiments.[9−11,13,14]

The large change in the peroxide content resulting from the irradiation (Figure 5) appears to contradict the insignificant change in the measured O/C and H/C ratios (Figure 3). The ToF-AMS instrument relies on electron impact ionization of flash-vaporized particles, leading to extensive fragmentation, which makes the ToF-AMS results difficult to interpret in a chemical context. In particular, the O−O bonds in peroxides are relatively weak and are likely fragmented completely in the ToF-AMS. Coincidently, this fragmentation across the O−O bond is also expected to occur during photolysis. Therefore, changes in chemical composition may be underestimated by the ToF-AMS method in situations when SOA aging is driven by condensed-phase photolysis.

BROADER IMPLICATIONS

Our experiments suggest that α-pinene ozonolysis SOA is photolabile on atmospherically relevant time scales. Experimental measurements of chemical composition and particle size indicate that excess ozone and high-volatility organic vapors do not appreciably participate in the photoinduced aging of α-pinene ozonolysis SOA. The condensed-phase processes, in particular the irradiation of particle-bound peroxides, appear to play the dominant role in α-pinene ozonolysis SOA aging. The applicability of this important result to other SOA model systems will definitively need to be verified in future experiments.

The peroxide content of SOA was found to be highly sensitive to UV exposure, which is reasonable considering the modestly high absorption cross sections and high photolysis quantum yields of peroxides.[28] Peroxides are abundant in all SOA produced by the ozonolysis of unsaturated organics, such as isoprene[19] and monoterpenes.[4] Therefore, condensed-phase irradiation of peroxides may induce significant changes in chemical composition and physical properties of biogenic SOA. Indeed, the primary step in the photolytic destruction of peroxides is formation of alkoxyl and hydroxyl radicals (reactions 1 and 2),[12] which are highly reactive and could potentially start a complex chain of radical-driven condensed-phase processes. Such reactions may induce fragmentation of SOA compounds, leading to volatilization, but may also form oligomers or less-volatile products that remain in the condensed-phase.

Roughly, 50% of the initial peroxide content remains after 1 week of exposure to sunlight at 34° latitude in the summer. While specific processes may add to the particle peroxide content, the peroxide lifetime that we have measured reflects the net change in peroxide molecules during UV exposure. Within the best-estimate mean particle age of 4−7 days,[29] irradiation has the potential to significantly deplete the particle peroxide content. Figure S11 details how the peroxide lifetime due to photolysis scales with the month of the year. The largest effects are expected in the summer; the peroxide lifetime due to irradiation during the late autumn and winter becomes too long to affect the chemical composition of SOA during its typical atmospheric lifetime.

We should point out that the destruction of peroxides by irradiation occurs on similar time scales as the aging of organic particles by OH radical, which typically serves as the main driver of atmospheric oxidation processes. Chemical lifetimes due to OH aging of aerosol are highly dependent on the species of interest and the particle size. For a 500 nm particle, the effective OH rate constant will be 1×10^{-12} cm^3 molecule^{-1} s^{-1},[30] leading to an effective oxidation lifetime of 5.8 days at the globally averaged OH concentration value of 2×10^6 molecules cm^{-3}.

Peroxide-laden PM has been shown to induce adverse health effects in rats upon inhalation.[31] Venkatachari and Hopke[32] propose that peroxides produced in the ozonolysis of α-pinene could deliver reactive oxygen species *in vivo* to tissue. Since particle-bound peroxides are highly photolabile, photolytic aging may act to pacify some of the adverse health effects of inhaling peroxide-laden PM.

■ ASSOCIATED CONTENT

Supporting Information

A plot confirming complete ozone removal by the denuders (Figure S1); PTR-ToF-MS data showing the removal of VOCs by the denuders and the change in VOC concentrations upon irradiation (Figure S2); the potential effects of temperature on SOA composition inside the flow cells (Figure S3); calculations quantifying the UV-light spectral flux density inside the flow cell (Figures S4−S9 and eqs S1−S4); aerosol heat transfer calculations proving that evaporation from particle heating is negligible in these experiments (eqs S5−S13); average O/C ratio of SOA in cases A, B, and C (Figure S10); and estimated aerosol peroxide lifetimes in Los Angeles, CA throughout the year (Figure S11). This material is available free of charge via the Internet at http://pubs.acs.org/.

■ AUTHOR INFORMATION

Corresponding Author

*Phone: (949) 824-1262. Fax: (949) 824-8571. E-mail: nizkorod@uci.edu.

Notes

The authors declare no competing financial interest.

■ ACKNOWLEDGMENTS

Funding from NSF grants AGS-1227579 (S.A.N.) and NSF CHE-0909227 (S.A.E. and S.L.B.) are acknowledged. The PTR-ToF-MS and ToF-AMS instruments were acquired with help of the NSF grant MRI-0923323.

■ REFERENCES

(1) Zhang, Q.; Jimenez, J. L.; Canagaratna, M. R.; Allan, J. D.; Coe, H.; Ulbrich, I.; Alfarra, M. R.; Takami, A.; Middlebrook, A. M.; Sun, Y. L.; Dzepina, K.; Dunlea, E.; Docherty, K.; DeCarlo, P. F.; Salcedo, D.; Onasch, T.; Jayne, J. T.; Miyoshi, T.; Shimono, A.; Hatakeyama, S.; Takegawa, N.; Kondo, Y.; Schneider, J.; Drewnick, F.; Borrmann, S.; Weimer, S.; Demerjian, K.; Williams, P.; Bower, K.; Bahreini, R.; Cottrell, L.; Griffin, R. J.; Rautiainen, J.; Sun, J. Y.; Zhang, Y. M.; Worsnop, D. R. Ubiquity and dominance of oxygenated species in organic aerosols in anthropogenically-influenced Northern Hemisphere midlatitudes. *Geophys. Res. Lett.* **2007**, *34* (13), L13801.

(2) Hallquist, M.; Wenger, J. C.; Baltensperger, U.; Rudich, Y.; Simpson, D.; Claeys, M.; Dommen, J.; Donahue, N. M.; George, C.; Goldstein, A. H.; Hamilton, J. F.; Herrmann, H.; Hoffmann, T.; Iinuma, Y.; Jang, M.; Jenkin, M. E.; Jimenez, J. L.; Kiendler-Scharr, A.; Maenhaut, W.; McFiggans, G.; Mentel, T. F.; Monod, A.; Prévôt, A. S. H.; Seinfeld, J. H.; Surratt, J. D.; Szmigielski, R.; Wildt, J. The formation, properties and impact of secondary organic aerosol: current and emerging issues. *Atmos. Chem. Phys.* **2009**, *9* (14), 5155−5236.

(3) Kroll, J. H.; Seinfeld, J. H. Chemistry of secondary organic aerosol: Formation and evolution of low-volatility organics in the atmosphere. *Atmos. Environ.* **2008**, *42* (16), 3593−3624.

(4) Docherty, K. S.; Wu, W.; Lim, Y. B.; Ziemann, P. J. Contributions of Organic Peroxides to Secondary Aerosol Formed from Reactions of Monoterpenes with O_3. *Environ. Sci. Technol.* **2005**, *39* (11), 4049−4059.

(5) Surratt, J. D.; Murphy, S. M.; Kroll, J. H.; Ng, N. L.; Hildebrandt, L.; Sorooshian, A.; Szmigielski, R.; Vermeylen, R.; Maenhaut, W.; Claeys, M.; Flagan, R. C.; Seinfeld, J. H. Chemical Composition of Secondary Organic Aerosol Formed from the Photooxidation of Isoprene. *J. Phys. Chem. A* **2006**, *110* (31), 9665−9690.

(6) Russell, L. M.; Bahadur, R.; Ziemann, P. J. Identifying organic aerosol sources by comparing functional group composition in chamber and atmospheric particles. *Proc. Natl. Acad. Sci. U. S. A.* **2011**, *108* (9), 3516−3521.

(7) Koop, T.; Bookhold, J.; Shiraiwa, M.; Poschl, U. Glass transition and phase state of organic compounds: dependency on molecular properties and implications for secondary organic aerosols in the atmosphere. *Phys. Chem. Chem. Phys.* **2011**, *13* (43), 19238−19255.

(8) Presto, A. A.; Huff Hartz, K. E.; Donahue, N. M. Secondary Organic Aerosol Production from Terpene Ozonolysis. 1. Effect of UV Radiation. *Environ. Sci. Technol.* **2005**, *39* (18), 7036−7045.

(9) Mang, S. A.; Henricksen, D. K.; Bateman, A. P.; Andersen, M. P. S.; Blake, D. R.; Nizkorodov, S. A. Contribution of Carbonyl Photochemistry to Aging of Atmospheric Secondary Organic Aerosol. *J. Phys. Chem. A* **2008**, *112* (36), 8337−8344.

(10) Pan, X.; Underwood, J. S.; Xing, J. H.; Mang, S. A.; Nizkorodov, S. A. Photodegradation of secondary organic aerosol generated from limonene oxidation by ozone studied with chemical ionization mass spectrometry. *Atmos. Chem. Phys.* **2009**, *9* (12), 3851−3865.

(11) Walser, M. L.; Park, J.; Gomez, A. L.; Russell, A. R.; Nizkorodov, S. A. Photochemical Aging of Secondary Organic Aerosol Particles Generated from the Oxidation of d-Limonene. *J. Phys. Chem. A* **2007**, *111* (10), 1907−1913.

(12) Kroll, J. H.; Ng, N. L.; Murphy, S. M.; Flagan, R. C.; Seinfeld, J. H. Secondary Organic Aerosol Formation from Isoprene Photooxidation. *Environ. Sci. Technol.* **2006**, *40* (6), 1869−1877.

(13) Bateman, A. P.; Nizkorodov, S. A.; Laskin, J.; Laskin, A. Photolytic processing of secondary organic aerosols dissolved in cloud droplets. *Phys. Chem. Chem. Phys.* **2011**, *13* (26), 12199−12212.

(14) Nguyen, T. B.; Laskin, A.; Laskin, J.; Nizkorodov, S. A. Direct aqueous photochemistry of isoprene high-NOx secondary organic aerosol. *Phys. Chem. Chem. Phys.* **2012**, *14* (27), 9702−9714.

(15) Ludwig, B. E.; McMillan, G. R. Primary quantum yields in photodissociation of isopropyl nitrite. *J. Am. Chem. Soc.* **1969**, *91* (5), 1085−1088.

(16) Vaden, T. D.; Imre, D.; Beránek, J.; Shrivastava, M.; Zelenyuk, A. Evaporation kinetics and phase of laboratory and ambient secondary organic aerosol. *Proc. Natl. Acad. Sci. U. S. A.* **2011**, *108* (6), 2190−2195.

(17) Lambe, A. T.; Zhang, J.; Sage, A. M.; Donahue, N. M. Controlled OH Radical Production via Ozone-Alkene Reactions for Use in Aerosol Aging Studies. *Environ. Sci. Technol.* **2007**, *41* (7), 2357−2363.

(18) Banerjee, D. K.; Budke, C. C. Spectrophotometric Determination of Traces of Peroxides in Organic Solvents. *Anal. Chem.* **1964**, *36* (4), 792−796.

(19) Nguyen, T. B.; Bateman, A. P.; Bones, D. L.; Nizkorodov, S. A.; Laskin, J.; Laskin, A. High-resolution mass spectrometry analysis of secondary organic aerosol generated by ozonolysis of isoprene. *Atmos. Environ.* **2010**, *44* (8), 1032−1042.

(20) Ziemann, P. J. Aerosol products, mechanisms, and kinetics of heterogeneous reactions of ozone with oleic acid in pure and mixed particles. *Faraday Discuss.* **2005**, *130*, 469−490.

(21) Mutzel, A.; Rodigast, M.; Iinuma, Y.; Böge, O.; Herrmann, H. An improved method for the quantification of SOA bound peroxides. *Atmos. Environ.* **2013**, *67*, 365−369.

(22) Misra, C.; Singh, M.; Shen, S.; Sioutas, C.; Hall, P. M. Development and evaluation of a personal cascade impactor sampler (PCIS). *J. Aerosol Sci.* **2002**, *33* (7), 1027−1047.

(23) Awtrey, A. D.; Connick, R. E. The Absorption Spectra of I_2, I_3^-, I^-, IO_3^-, $S_4O_6^=$ and $S_2O_3^=$. Heat of the Reaction $I_3^- = I_2 + I^-$. *J. Am. Chem. Soc.* **1951**, *73* (4), 1842−1843.

(24) Monge, M. E.; Rosenørn, T.; Favez, O.; Müller, M.; Adler, G.; Abo Riziq, A.; Rudich, Y.; Herrmann, H.; George, C.; D'Anna, B. Alternative pathway for atmospheric particles growth. *Proc. Natl. Acad. Sci. U. S. A.* **2012**, *109*, 6840−6844.

(25) Hung, H.-M.; Chen, Y.-Q.; Martin, S. T. Reactive aging of films of secondary organic material studied by infrared spectroscopy. *J. Phys. Chem. A* **2013**, *117* (1), 108−116.

(26) Kamboures, M. A.; Nizkorodov, S. A.; Gerber, R. B. Ultrafast photochemistry of methyl hydroperoxide on ice particles. *Proc. Natl. Acad. Sci. U. S. A.* **2010**, *107* (15), 6600−6604.

(27) Finlayson-Pitts, B. J.; Pitts, J. N. *Chemistry of the Upper and Lower Atmosphere: Theory, Experiments, and Applications*; Academic Press: 2000.
(28) Epstein, S. A.; Shemesh, D.; Tran, V. T.; Nizkorodov, S. A.; Gerber, R. B. Absorption Spectra and Photolysis of Methyl Peroxide in Liquid and Frozen Water. *J. Phys. Chem. A* **2012**, *116* (24), 6068−6077.
(29) Rudich, Y.; Donahue, N. M.; Mentel, T. F. Aging of Organic Aerosol: Bridging the Gap Between Laboratory and Field Studies. *Annu. Rev. Phys. Chem.* **2007**, *58* (1), 321−352.
(30) Donahue, N. M.; Chuang, W.; Epstein, S. A.; Kroll, J. H.; Worsnop, D. R.; Robinson, A. L.; Adams, P. J.; Pandis, S. N. Why do organic aerosols exist? Understanding aerosol lifetimes using the two-dimensional volatility basis set. *Environmental Chemistry* **2013**, *10* (3), 151−157.
(31) Morio, L. A.; Hooper, K. A.; Brittingham, J.; Li, T.-H.; Gordon, R. E.; Turpin, B. J.; Laskin, D. L. Tissue Injury Following Inhalation of Fine Particulate Matter and Hydrogen Peroxide Is Associated with Altered Production of Inflammatory Mediators and Antioxidants by Alveolar Macrophages. *Toxicol. Appl. Pharmacol.* **2001**, *177* (3), 188−199.
(32) Venkatachari, P.; Hopke, P. K. Characterization of products formed in the reaction of ozone with α-pinene: case for organic peroxides. *Journal of Environmental Monitoring* **2008**, *10* (8), 966−974.